Journal of Catalysis **186,** 20–30 (1999)
Article ID jcat.1999.2461, available online at http://www.idealibrary.com on IDEAL®

Evidence of Alloy Formation during the Activation of Graphite-Supported Palladium-Cobalt Catalysts

F. B. Noronha,*[,1] M. Schmal,* R. Fréty,† G. Bergeret,‡ and B. Moraweck‡[,2]

*NUCAT-COPPE/EQ, Universidade Federal do Rio de Janeiro, Ilha do Fundão, Bl.G, C.P. 68502, CEP 21941, Rio de Janeiro, Brazil; †Laboratoire d'Application de la Chimie à l'Environnement, CNRS, 43 Boulevard du 11 Novembre 1918, F 69622 Villeurbanne Cedex, France; and ‡Institut de Recherches sur la Catalyse, CNRS, 2 Avenue Albert Einstein, F 69626, Villeurbanne Cedex, France

Received September 23, 1998; revised February 18, 1999; accepted February 18, 1999

Magnetism, XRD, and EXAFS analyses were used to study the formation of a solid solution on Pd-Co/G catalysts during reduction treatment. After reduction at 773 K, magnetic measurements revealed the formation of a Pd-Co alloy. XRD analysis *in situ* allowed us to follow the alloy process during the increase of the reduction temperature. The XRD results showed the presence of a heterogeneous solid solution after reduction at 773 K. Pd and Co K-edge EXAFS analysis confirmed that bimetallic particles with a palladium- and cobalt-rich phase were formed. The formation of a solid solution decreased the adsorption strength of 1,3-butadiene on new Pd sites modified by Co.

Key Words: **cobalt; palladium; graphite; bimetallic catalysts; *in situ* XRD; EXAFS; magnetization; alloy formation.**

1. INTRODUCTION

It is well known that the addition of a second metal to a metallic-supported catalyst creates important changes in catalytic and adsorptive properties (1–4). For example, the addition of a noble metal (Pd, Pt) to iron or cobalt catalysts increases the selectivity for methanol formation from synthesis gas at high pressure (5–8). Woo *et al.* (6) attributed such an increase to the presence of a FePt alloy phase. According to Guczi (7), alloy formation could affect both hydrogen and carbon monoxide adsorption and thereby activity and selectivity. On silica-supported Pt-Co catalysts, a strong enhancement in the hydrogenolysis selectivity as the cobalt content increased was explained by the presence of unalloyed Co, by a Co-rich phase, or by segregation of cobalt at the surface (9).

Although numerous studies have been devoted to Pd-Co catalysts (10–13), the exact role of Pd on the evolution of the properties of cobalt still needs to be better defined, as well as the degree of interaction between both metals. In general, it is ascribed that the addition of palladium promotes the reduction of cobalt oxide (14–17) by the activation of hydrogen on metallic palladium followed by the migration of the activated hydrogen to cobalt oxide (14–16). For example, Kapoor *et al.* (15) observed a strong increase in the reducibility of Co/Al_2O_3 catalysts upon the addition of palladium. The addition of palladium to Co/CeO_2 catalysts induced the formation of ethanol in $CO + H_2$ reaction (14). TPR analysis suggests an intimate contact between both metals. However, no direct evidence about alloy formation is presented and the mechanism of the alloying is not described.

Recently, the present authors have followed the reduction of Pd-Co catalyst by TPR and electron-microscopy (17). A mechanism for the bimetallic formation was proposed. We showed that on the graphite-supported Pd-Co catalyst, two mechanisms take place. As revealed by TEM, an intimate contact between both oxide particles and the motion of the particles can explain the promoting effect of the metallic palladium on the cobalt oxide reduction. However, no direct evidence about alloy formation was obtained by using these techniques.

In the present paper, we performed *in situ* X-ray diffraction experiments in order to verify the formation of Pd-Co solid solutions after the reducing treatment. An additional EXAFS study at both Pd and Co K-edge was also carried out to determine the order at an atomic scale.

2. EXPERIMENTAL

2.1. Catalyst Preparation

A graphite (Lonza, HSAG II; BET area: 130 m^2/g) was used as support. The monometallic and bimetallic catalysts were prepared by the incipient wetness impregnation of the support with an aqueous solution of $Pd(NO_3)_2 \cdot 2H_2O$ (STREM Chemicals) and $Co(NO_3)_2 \cdot 6H_2O$ (Merck), followed by drying at 393 K for 16 h and calcination in air at 673 K for 2 h. The prepared catalysts and their metal contents are presented in Table 1.

[1] Present address: Instituto Nacional de Tecnologia, Av. Venezuela 82, CEP 20081-310, Rio de Janeiro, Brazil. Fax: (55-21) 263 6552.

[2] To whom correspondence should be addressed. E-mail: moraweck@catalyse.univ-lyon1.fr.

0021-9517/99 $30.00

TABLE 1

Catalyst Composition (Pd_xCo_y: x and y Represent the Atomic Percentage of Pd and Co Deduced from Chemical Analysis)

	Composition (wt%)	
Catalyst	Pd	Co
Pd/G	2.26	
$Pd_{33}Co_{67}$/G	3.12	3.44
$Pd_{16}Co_{84}$/G	3.37	9.96
Co/G		3.61

2.2. Magnetic Measurements

The magnetic experiments and equipment were described previously (17). The catalysts were reduced at 873 K under a flowing mixture of 1% hydrogen in argon. After reduction, magnetic measurements were performed to verify the formation of a Pd-Co alloy. The magnetization was measured at 298 K, using the extraction method of Weiss (18, 19). Saturation magnetization (M_S) was obtained by plotting the magnetization M against $1/H$ (H = magnetic field) and extrapolating to $1/H = 0$. M_S allowed the calculation of the magnetic moment associated with the atom of alloy.

2.3. X-Ray Diffraction (XRD)

X-ray diffraction patterns were obtained with a D500 Siemens goniometer using Zr filtered Mo$K\alpha$ radiation (0.71073 Å). A high temperature camera was used to follow the *in situ* reduction of the calcined precursors, without exposure to air, and the formation of the solid solution (20). The reducing gas was a mixture of 1% hydrogen in helium in order to work under conditions similar to those used in TPR (17). The data were recorded using a position-sensitive proportional counter (Raytech) in scanning mode ($\Delta 2\theta = 0.032^\circ$) and processed with the Diffract-AT software (Siemens-Socabim).

Crystallite sizes were estimated from the integral breadth of the lines using the Scherrer equation (21). The unit cell parameter was calculated from the measured interplanar spacing of the (200) and (220) reflections. The composition of each alloy was estimated by comparing the calculated lattice parameter with literature data of lattice constant as a function of the composition (22, 23).

2.4. Extended X-Ray Absorption Fine Structure (EXAFS)

EXAFS measurements were carried out on the D44 synchrotron beam line (DCI-LURE) with the storage ring operating at 1.85 GeV and a mean current of 250 mA. The experiments were performed in transmission mode at both Pd and Co K-edges, with a double Si (311) crystal monochromator. At the Co K-edge a double glass mirror device was inserted to eliminate high order harmonics. The pure palladium and bimetallic-reduced catalysts were transferred under dry nitrogen in a glove box in sealed containers without contacting air. The analysis of Co/G catalyst was performed *in situ* using the same reducing mixture as that in the XRD experiments.

The EXAFS spectra were recorded over a 1000 eV energy range with an energy step of 3 eV. Three to six spectra were added before they were analyzed in a standard manner (24). After background removal, the atomic-like absorption coefficient was obtained by fitting a polynomial of a convenient degree and was subsequently normalized using the method by Lengeler-Eisenberger (25). The k^3 weighted $\chi(k)$ function was then Fourier-transformed from $k = 3$ to 13 Å^{-1} using a Kaiser window ($t = 9$). The peak corresponding to the first coordination sphere was then isolated and back-Fourier-transformed into k space to determine the mean coordination number, n, the bond-length, R, and the Debye-Waller-like factor σ by a fitting procedure using the simplex method (26). Pd and Co foils (15 and 4 mm thick, respectively) were used to extract the backscattering amplitude and phase functions for the Pd-Pd and Co-Co pairs, respectively. For the Pd-Co and Co-Pd pairs, the results of the theoretical work by McKale *et al*. were used (27).

The quality of the fit was determined by a reliability factor defined as (20)

$$Q = \sum_i \frac{\left[k^3\left(\left|\chi_i^c(k)\right| - \left|\chi_i^e(k)\right|\right)\right]^2}{\left(k^3\chi_i^e(k)\right)^2}.$$

2.5. Hydrogen Chemisorption

The chemisorption uptakes were measured in a volumetric apparatus. The catalysts were reduced at 773 K in flowing H_2 (30 cm^3/min). Following reduction, the samples were evacuated, for 1 h, at reduction temperature and cooled to adsorption temperature under vacuum. Irreversible uptakes were determined from dual isotherms measured at 398 K since the hydrogen chemisorption on cobalt catalysts is activated (28).

2.6. Butadiene Hydrogenation

The butadiene hydrogenation was performed in a microreactor at atmospheric pressure and different temperatures. Catalyst mass was varied between 5 and 50 mg to keep conversions below 10%. The catalysts were diluted in silica (ratio 1/30) and reduced *in situ*, passing a mixture of 1.5% H_2/N_2 at 30 ml/min and raising the temperature at 10 K/min up to 773 K. Then, the sample was cooled and held at the reaction temperature. The gas mixture was switched to the reactant mixture of 1,3-butadiene/H_2/N_2 at a ratio of 10/10/80, flowing through the reactor at different flow rates. The products were analyzed by GC on line using a Carbopack C/0.19% picric acid column maintained at 313 K.

3. RESULTS

3.1. Magnetic Measurements

Figure 1 shows the ferromagnetic moments per atom of alloy as a function of the alloy composition for Co/G and the Pd-Co/G samples. Data of Pd-Co unsupported alloys obtained by Bozorth *et al.* (22) are also presented for comparison (black line). The magnetic moment of the catalysts fits the curve well based on the values of Pd-Co bulk alloys.

3.2. X-Ray Diffraction

After calcination, the diffraction patterns of the graphite-supported Pd, Co, and Pd-Co catalysts showed only the Bragg lines of PdO and Co_3O_4, which indicated the absence of mixed oxides in the precursor of the bimetallic catalyst (17).

Figure 2 shows the diffraction patterns of Pd, $Pd_{33}Co_{67}$, $Pd_{16}Co_{84}$, and Co reduced at 298 K (lower curve), 473 K (middle curve), and 773 K (upper curve).

For pure Co/G catalysts after reduction at 298 K, only the Bragg lines characteristic of the Co_3O_4 phase were present. With an increase of the reduction temperature, the Co_3O_4 lines disappeared and the lines corresponding to CoO were detected. After reduction at 773 K, only the Co metal lines were observed.

The pattern of pure Pd/G catalyst displayed the metallic palladium Bragg lines from 298 K. They increased upon heating at 473 and 773 K.

The bimetallic catalysts reduced at 298 K displayed the Pd (111) reflection. In the case of the Co-rich sample, the Bragg lines corresponding to Co_3O_4 were present beside the Pd (111) line. After reduction at 473 K, both the Pd (111) and Co (111) line were observed. These lines disappeared at 773 K and a new peak located between the Bragg lines of pure Pd and Co appeared on the diffraction pattern of the bimetallic catalysts.

Figure 3 exhibits the X-ray diffraction patterns recorded after reduction at 973 K and subsequent cooling at 300 K under H_2 (dashed curves) and under He (full curves) flow for the pure Pd and the bimetallic catalysts. For Pd/G, the peaks characteristic of metallic palladium shifted to lower 2θ values in a hydrogen atmosphere. On the other hand, for Co/G (not shown here) and bimetallic samples, the patterns under He or H_2 are identical.

3.3. EXAFS

Figure 4 displays the k^3 Fourier transform (FT) of the EXAFS functions at the Pd K-edge of the Pd/G and $Pd_{16}Co_{84}$/G catalyst after reduction at 773 K and of the standard Pd foil. The radial distribution functions (RDF)

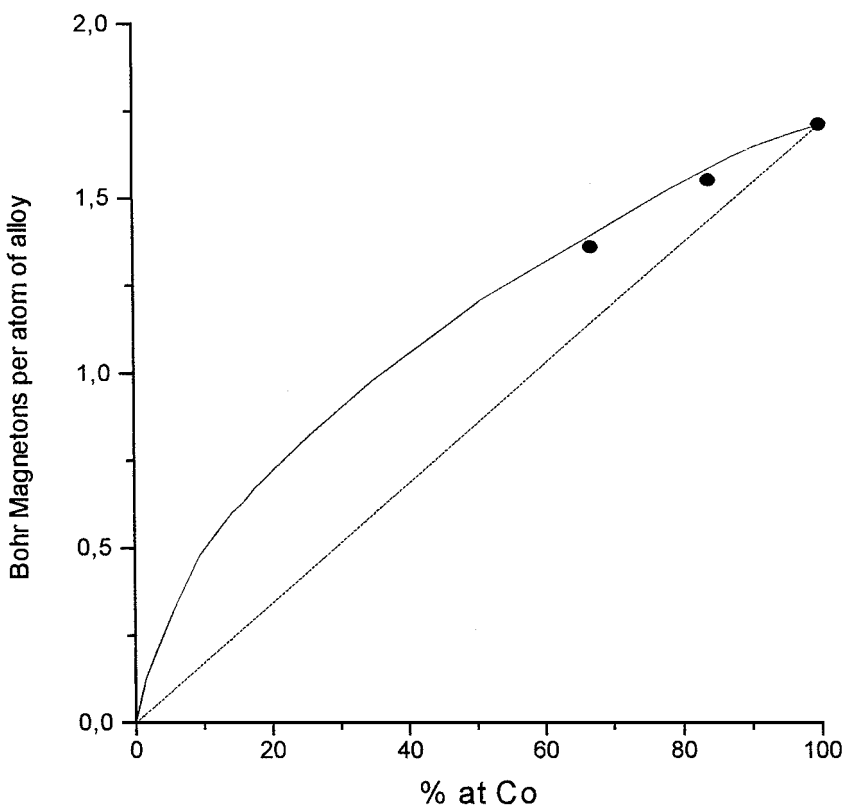

FIG. 1. Ferromagnetic moments per atom of alloy as a function of Co compostion: (●) Pd-Co/G catalysts; (—) Data of Pd-Co-unsupported alloys by Bozorth *et al.* (22).

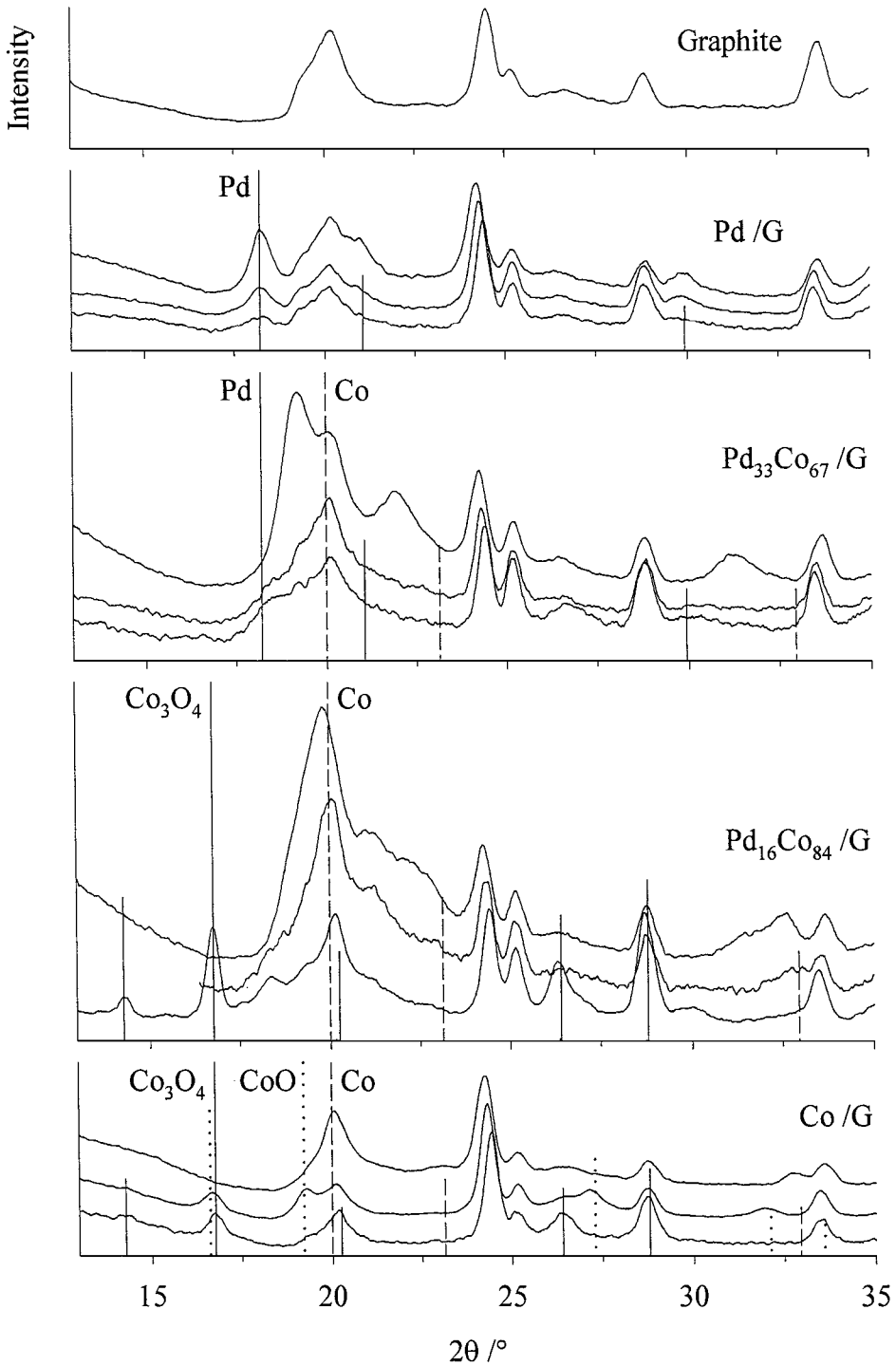

FIG. 2. X-ray diffraction patterns of the graphite carrier and monometallic and bimetallic catalysts after reduction at 293 K (lower curve), 473 K (middle curve), and 773 K (upper curve). Vertical bars indicate the position of the Bragg peaks for Pd, Co, Co_3O_4, and CoO extracted from the ICDD-Powder Diffraction File database.

were not corrected for phase shifts so that the observed peaks are shifted to lower *R* values from the true interatomic distances. There is one peak located at 2.45 Å in the RDF of the Pd foil and Pd/G catalyst which corresponds to the first coordination shell of Pd. On the other hand, on the $Pd_{16}Co_{84}$/G catalyst this peak is shifted toward a lower distance. The inverse Fourier transform of this peak for $Pd_{16}Co_{84}$/G catalysts is shown as the solid curve in Fig. 5. The results corresponding to the various fits in the k-space are summarized in Table 2.

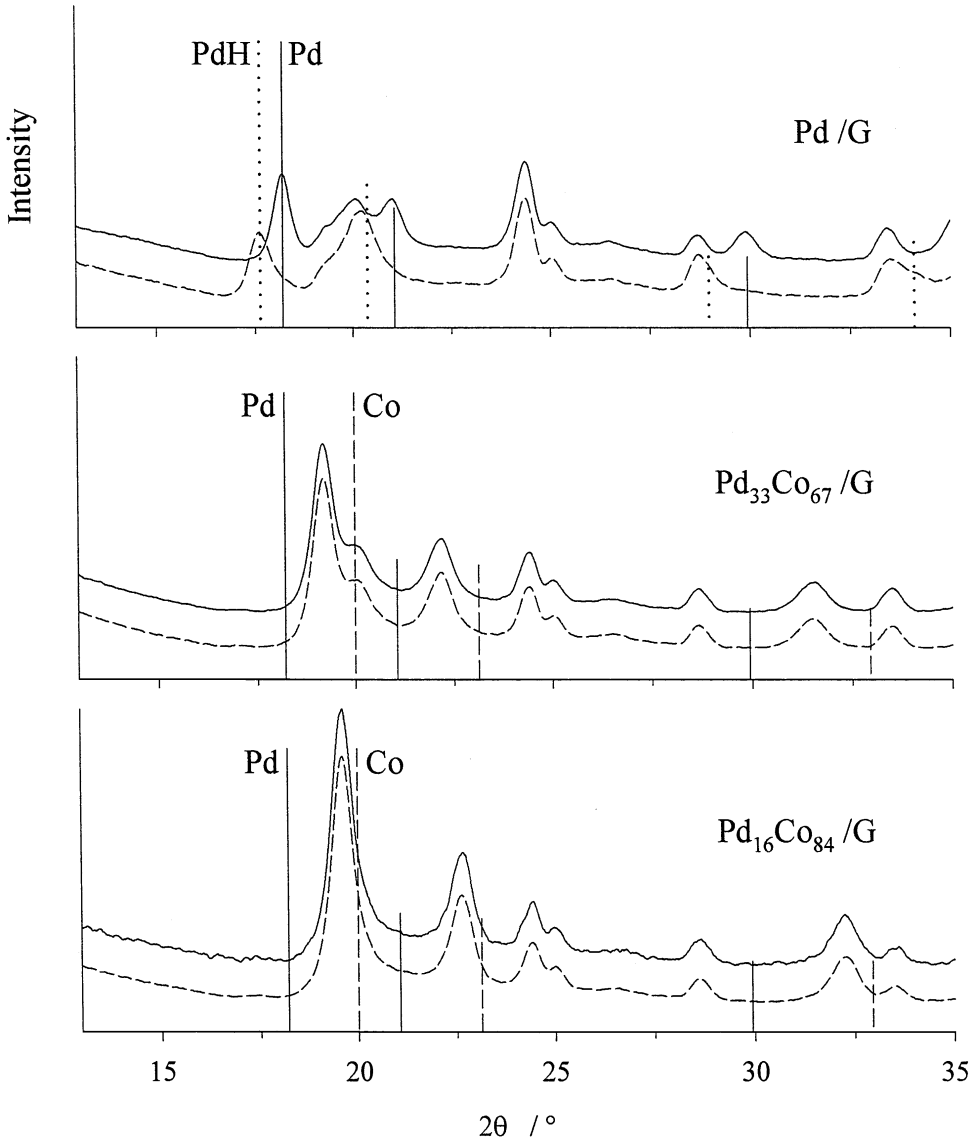

FIG. 3. X-ray patterns after reduction at 973 K and subsequent cooling at 300 K under H_2 (dashed line) or under He (full curve) for Pd monometallic, $Pd_{33}Co_{67}$/G, and $Pd_{16}Co_{84}$/G catalysts. Dotted, full, and dashed vertical lines indicate PdH hydride, Pd, and Co metals, respectively.

Figure 6 displays the RDFs resulting from Fourier transformation of the EXAFS function at the Co K-edge for Co/G, $Pd_{16}Co_{84}$/G, and Co foil. There is only one peak at around 2.5 Å (before phase correction) in the RDF of these samples. The inversed Fourier transforms of the RDF for $Pd_{16}Co_{84}$/G catalyst are displayed in Fig. 7. The structural parameters obtained by modeling the first coordination sphere at the Co K-edge are listed in Table 3.

TABLE 2

EXAFS Parameters at the Pd K-Edge

	Pd-Pd pair			Pd-Co pair				
Sample	n_1	R_1 (Å)	$\Delta\sigma^2$ (Å^2)	n_2	R_2 (Å)	$\Delta\sigma^2$ (Å^2)	Q (%)	n_1+n_2
Pd 15 μm	12.0	2.75	—	—	—	—	—	—
Pd/G	9.1	2.74	0.0000	—	—	—	5	—
$Pd_{16}Co_{84}$/G	4.0	2.67	0.0004	6.5	2.61	0.0076	7	10.5

TABLE 3

EXAFS Parameters at the Co K-Edge

	Co-Co pair			Co-Pd pair				
Sample	n_1	R_1 (Å)	$\Delta\sigma^2$ (Å^2)	n_2	R_2 (Å)	$\Delta\sigma^2$ (Å^2)	Q (%)	n_1+n_2
Co 5 μm	12.0	2.51	—	—	—	—	—	—
Co/G	11.5	2.50	0.0020	—	—	—	3	11.5
$Pd_{16}Co_{84}$/G	8.0	2.50	0.0060	3.7	2.61	0.0080	9	11.7

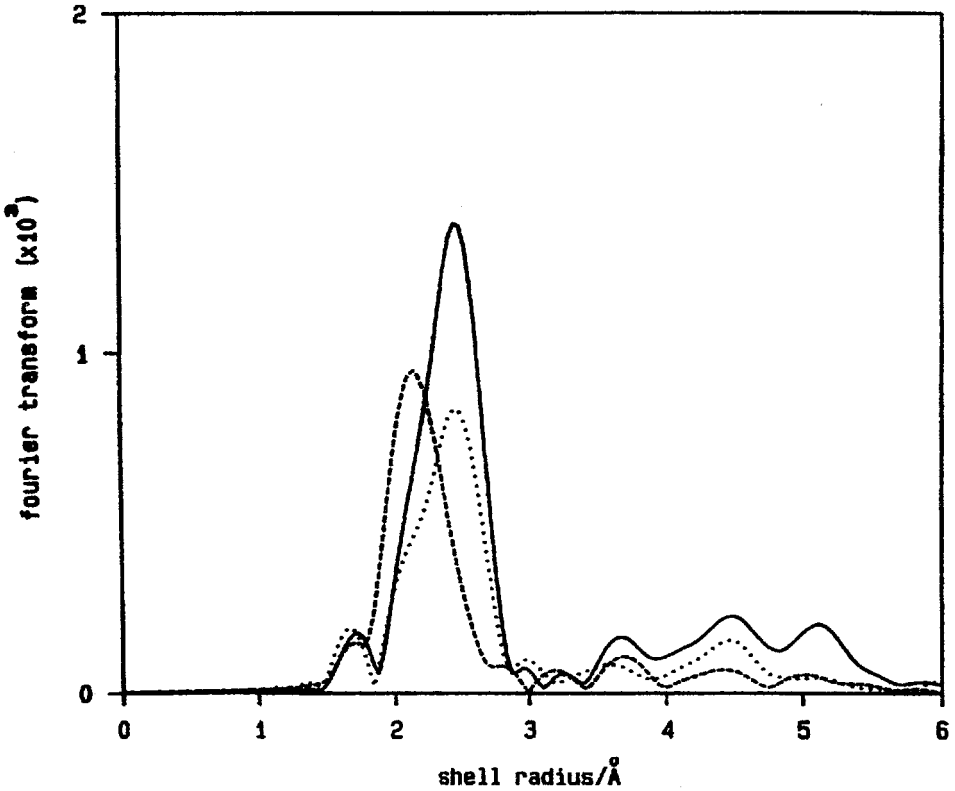

FIG. 4. Amplitude of the radial distribution function at the Pd K-edge for palladium foil (solid line) and Pd/G (dotted line) and $Pd_{16}Co_{84}$/G (dashed line).

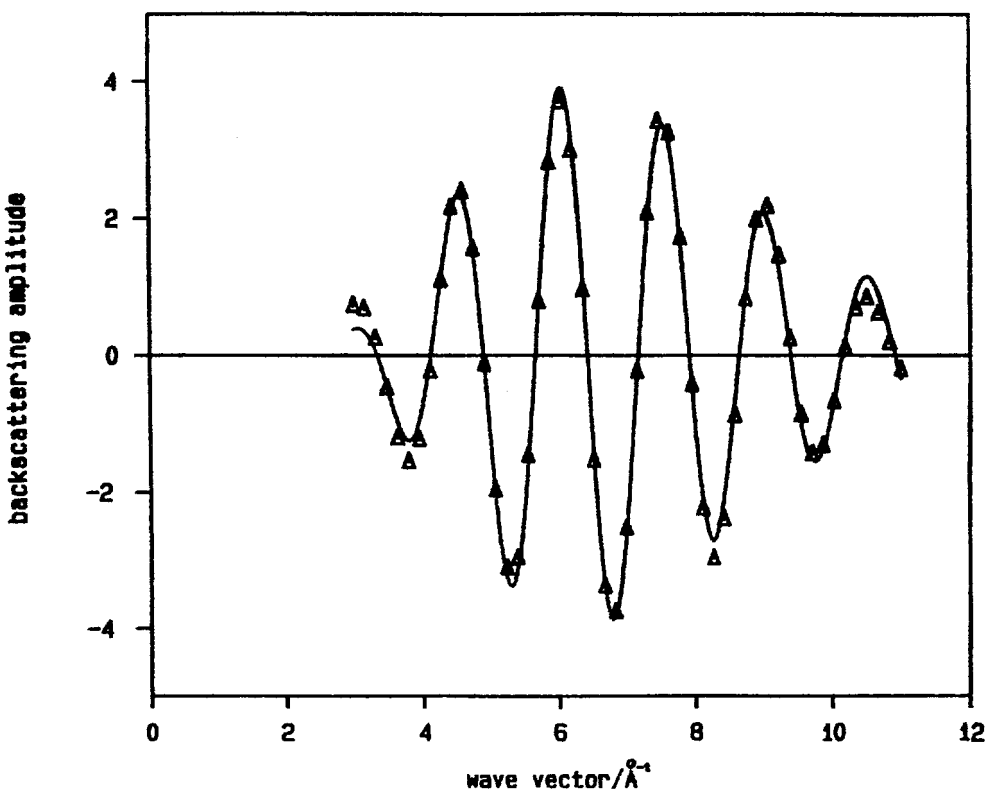

FIG. 5. Inverse Fourier transform of the first peak at the Pd K-edge for the $Pd_{16}Co_{84}$/G (solid line) and experimental points (triangles).

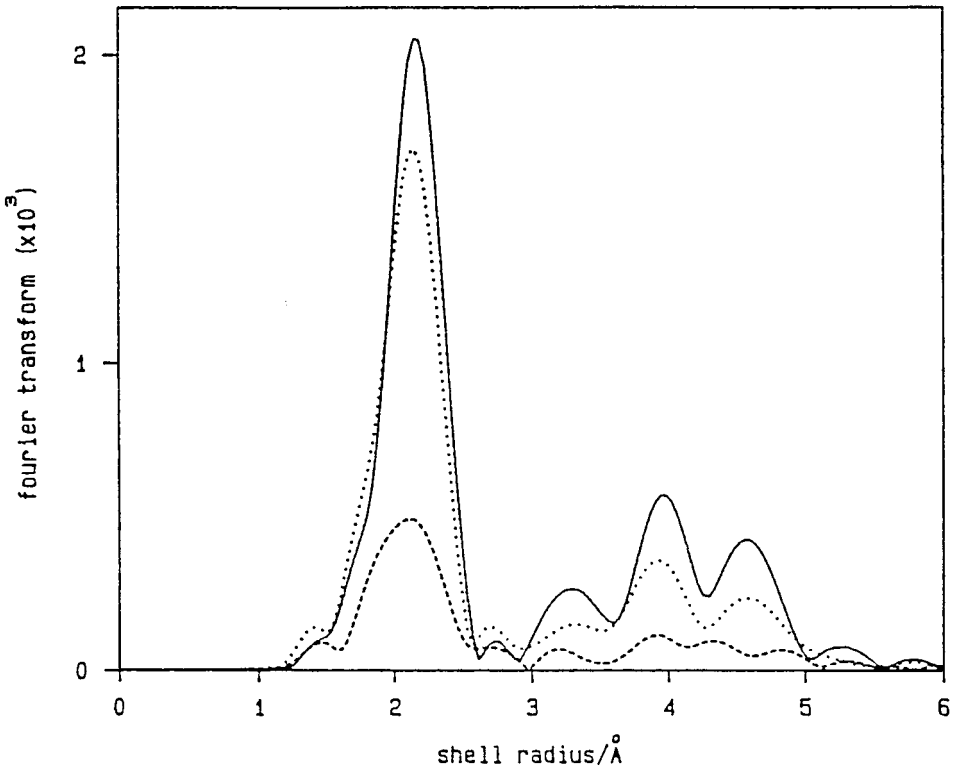

FIG. 6. Amplitude of the radial distribution function at the Co K-edge for cobalt foil (solid line) and Co/G (dotted line) and $Pd_{16}Co_{84}$/G (dashed line).

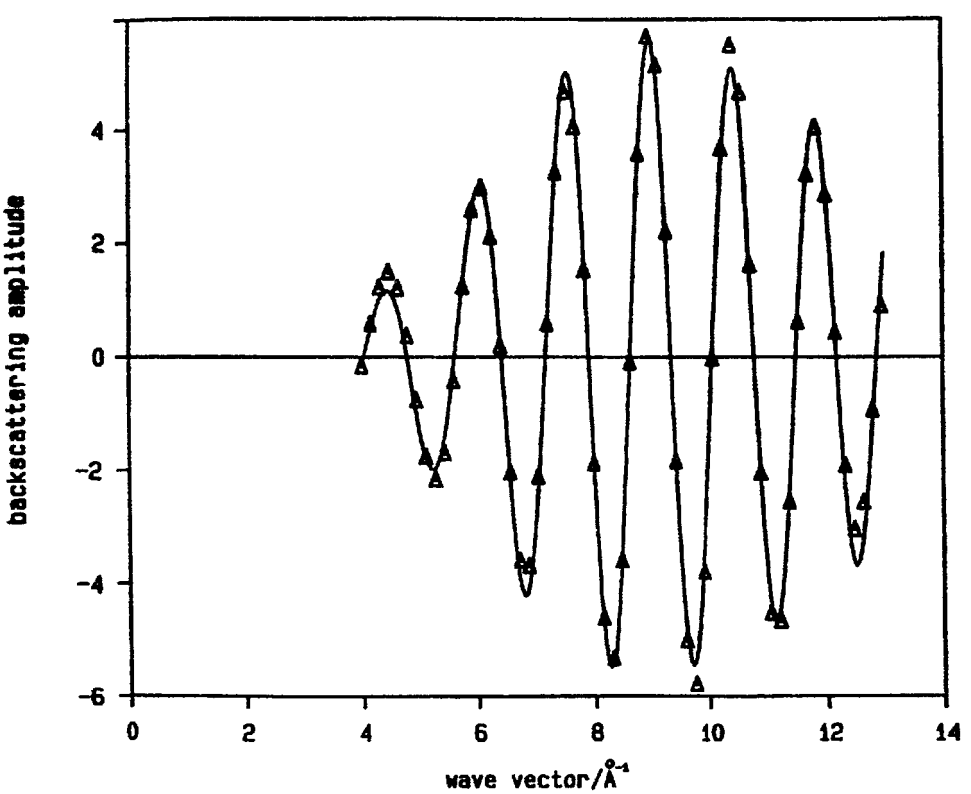

FIG. 7. Inverse Fourier transform of the first peak at the Co K-edge for the $Pd_{16}Co_{84}$/G (solid line) and experimental points (triangles).

TABLE 4

Catalytic and Selectivity Results of 1,3-Butadiene (BD) Hydrogenation on Pd-Co Catalysts[a]

Catalyst	Rate (gmol BD/g_{Metal} · s)	H_2 uptake (μmol H_2/g_{Metal})	TOF (s^{-1})	S_1 (%)	t/c
Pd/G	0.0023	145	2.9	52	6.7
$Pd_{33}Co_{67}$/G	0.0009	36	7.3	53	6.8
$Pd_{16}Co_{84}$/G	0.0018	50	8.7	57	4.5

[a] Reaction rate at 298 K (conversion, 5%); irreversible hydrogen adsorption; turnover frequency (TOF); selectivity toward 1-butene (S_1); *trans/cis* 2-butene ratio (t/c).

3.4. Butadiene Hydrogenation

The results of activity and selectivity for the bimetallic catalysts are presented in Table 4. The TOF values were calculated based on the irreversible hydrogen adsorption. The Co/G catalyst did not present any activity for the butadiene hydrogenation. On the other hand, the Pd-Co/G catalysts exhibited higher turnover frequencies when cobalt is added to the Pd/G sample. In addition, the selectivity toward 1-butene increased while the *trans/cis* ratio decreased.

4. DISCUSSION

One of the most important questions to be addressed when characterizing supported bimetallic catalysts is whether alloy particles are formed or not. In particular, palladium and cobalt form a continuous series of solid solutions (11, 12) and even ordered phases (Pd_3Co and PdCo) may be detected in bulk alloys (22, 23).

4.1. Magnetic Measurements

In a previous work (17), TPR results suggested that an interaction between Pd and Co exists on graphite-supported Pd-Co catalysts reduced at 873 K. But these results did not give clear evidence of alloy formation. Magnetic measurements are particularly valuable tools for obtaining such an information (19, 29, 30).

The experimental values in Fig. 1 lie above the theoretical straight line, which corresponds to a progressive dilution of the Pd network by Co. On the contrary, they are close to the experimental curve obtained by Bozorth *et al.* (22) for unsupported Pd-Co alloys. These authors proved that for diluted alloys of cobalt in palladium, the magnetization enhanced the magnetic moment borne by Co atoms, which induces a magnetic moment on the surrounding Pd atoms. This effect, called giant moment, is characteristic of Pd-Co and Pd-Fe alloys (31). Our experiments exhibited the same effect and it may be considered as a proof of an intimate contact between Pd and Co particles.

4.2. X-Ray Diffraction

After reduction at room temperature (Fig. 2), the pattern of the Co/G monometallic catalyst is similar to that obtained after the calcination step. Only the lines of the Co_3O_4 phase are detected. This indicates that cobalt is not reduced at this temperature, in agreement with TPR and magnetic results (17). After reduction at 473 K (Fig. 2), the Co_3O_4 lines vanished while the lines corresponding to the CoO phase appeared. This is supported by TPR results (17), which have shown that the reduction of Co_3O_4 to CoO occurs in this temperature range. Metallic cobalt was only present after reduction at 773 K (Fig. 2). A further increase of the temperature to 973 K (Fig. 2) led to an increase and a sharpening of the Co diffraction lines which indicate a sintering of the metal particles.

For the Pd/G sample reduced at room temperature (Fig. 2), the PdO lines disappeared and only a weak and broad line corresponding to the Pd (111) reflection was detected. This suggests that very small palladium particles have been formed after reduction at room temperature. Furthermore, the TPR profile of the Pd/G catalyst showed a hydrogen uptake at room temperature assigned to the reduction of palladium oxide. In the case of $Pd_{33}Co_{67}$ bimetallic sample (Fig. 2), the characteristic lines of the oxide phases (i.e., PdO and Co_3O_4) also disappeared and a shoulder corresponding to the Pd (111) line was observed. However, for the Co species, either CoO or Co metal could not be specified due to a superposition of the diffraction lines of the graphite. On the other hand, magnetic measurements and TPR results (17) revealed the presence of metallic cobalt. Therefore, the metallic cobalt was formed after reduction at room temperature and was probably either well dispersed or the concentration was too low to be identified by XRD. The pattern of the Co-rich bimetallic catalyst $Pd_{16}Co_{84}$/G (Fig. 2) displayed the lines corresponding to both metallic palladium and Co_3O_4. Nevertheless, after reduction at room temperature, the intensity of the cobalt oxide lines decreased in comparison to that in the calcined state (not shown here), suggesting that some reduction occurred at this temperature in the presence of palladium. Unfortunately, neither magnetism nor TPR experiments were able to support this point (17).

After reduction at 473 K, the pure Pd/G catalyst (Fig. 2) showed all the lines of metallic palladium, which implies quite an important sintering process. The increase of the particle size is probably due to an easy migration of metal particles over the smooth surface of graphite as seen by electron microscopy (17). The pattern of $Pd_{33}Co_{67}$ catalyst reduced at 473 K (Fig. 2) is close to the one obtained after reduction at room temperature (Fig. 2) with a broad Pd (111) line. However, the line at $2\theta = 20°$, corresponding to both the metallic Co (111) line and the graphite, increased. Therefore, a fraction of cobalt is reduced to the

metallic state at 473 K. For the $Pd_{16}Co_{84}$/G sample (Fig. 2), the lines of the cobalt oxide Co_3O_4 disappeared completely whereas metallic cobalt is clearly seen. The catalytic effect of palladium on the cobalt oxide reduction is more evident.

In the Pd/G sample reduced at 773 K, the sintering process of Pd particles, initiated at 473 K, is now strongly favored, as shown from the higher intensity of the metal lines (Fig. 2). For the bimetallic samples, the Pd-Co solid solution is evidenced by the appearance of new lines located between the lines of both pure metals (Fig. 2). The unit cell parameter of the solid solution, calculated from the position of the (111) line in the $2\theta = 18$–20° region, corresponds to a Pd mean atomic concentration of 34.4 and 5.9% for $Pd_{33}Co_{67}$ and $Pd_{16}Co_{84}$, respectively (20). Since the metal lines are partly polluted by the lines of graphite, these values must be considered only as indicative. Moreover, the important width of the diffraction lines indicates a distribution of particle composition and/or size. Indeed, EDX-STEM analysis on reduced and passivated catalysts revealed that Pd and Co are present in all particles but with both different compositions and particle sizes. We observed that small particles were enriched in palladium, whereas the larger ones were enriched in cobalt. Mallát *et al*. (13) also observed the presence of broad XRD lines in Pd-Co/C catalysts. According to them, all bimetallic catalysts were heterogeneous, presenting particles composed of Co or Co-rich disordered alloy in addition to a Pd-rich phase.

The reduction at 973 K (Fig. 3) led to a sintering of the bimetallic particles and a homogenization of the solid solution, as shown both by the sharpening of the peaks and by their intensity increase. The position of the (111) line leads to a Pd mean atomic concentration of 35.2 and 15.5%, in agreement with the chemical analysis (CA) of $Pd_{33}Co_{67}$ and $Pd_{16}Co_{84}$, respectively. The width of the (111) peak allowed estimates of 6 nm for the average size of the bimetallic particles (assuming tentatively that all the bimetallic particles have the same Pd-Co composition) and 9 nm for monometallic particles of Pd/G (Fig. 3). Therefore, the agreement between the composition values measured by XRD and CA indicates the formation of homogeneous bimetallic particles, after treatment at 973 K.

It is known that the β-hydride formation occurs on pure palladium in the presence of H_2 at 300 K (32). This is shown for Pd/G catalyst in Fig. 3. On the other hand, the bimetallic catalysts (Fig. 3) presented similar patterns under H_2 and under He atmosphere. Generally, β-hydride formation on alloys is more difficult when the second metal content is increased. This suggests the absence of pure Pd particles and the presence of a Pd-Co alloy. In addition, the TPR profile of the bimetallic catalyst (17) did not exhibit a negative peak ascribed to the β-hydride decomposition, which supports that both metals are in intimate contact.

4.3. EXAFS

Since Stern (33), Lytle *et al*. (34), Stern *et al*. (35), and Sinfelt *et al*. (36) developed the theory of EXAFS, numerous works have clearly demonstrated that the EXAFS technique is a valuable tool for obtaining structural information about the interaction of the two components of the bimetallic catalysts (36–40). In our work, EXAFS was used to obtain further evidence of a Pd-Co interaction and the mean composition of bimetallic particles.

As shown in Fig. 4, the RDF of bimetallic catalyst is different from the RDF of both Pd/G catalyst and reference sample. The curve fitting carried out with both Pd and Co atoms in the first coordination shell of Pd led to a good fit (Fig. 5). This means that the first coordination shell of palladium in the bimetallic catalyst and in the reference is different. The first coordination shell consists of palladium atoms alone in the Pd/G and in the reference even though it has both palladium and cobalt atoms in the bimetallic catalyst. Moreover, the total coordination number is 10.5 (Table 2), which is in agreement with the presence of rather large particles. The local atomic concentration of palladium, obtained by the $n_1/(n_1 + n_2)$ ratio (20), was 38%, suggesting that the first shell around Pd atoms is clearly palladium-enriched with respect to the catalyst chemical composition.

The RDF of the bimetallic catalyst is not so different from the RDF of both Co/G catalyst and reference (Fig. 6). This suggests that the environment of cobalt atoms in the $Pd_{16}Co_{84}$/G and in the reference sample is similar. However, since a fairly good fit cannot be obtained only with Co atoms in the first coordination sphere of cobalt, it was necessary to perform the fit with Pd and Co atoms (Fig. 7). This results in a mean palladium concentration of 32% around a Co atom, which is much larger than that expected from chemical analysis.

Therefore, the EXAFS analysis demonstrated that the bimetallic phase was formed during reduction, as already shown by magnetic and X-ray diffraction measurements. The bimetallic particles consist of both palladium- and cobalt-rich phases.

Consequently, two models could be proposed:

(i) the formation of bimetallic particles with a central core of cobalt surrounded by an outer layer rich in palladium;

(ii) the presence of bimetallic particles with different compositions such as rich and poor palladium particles.

On Pd-Co systems, theoretical calculations (41), and experimental results (16) have reported a surface enrichment of palladium. According to TEM experiments, if we assume that the particles of the bimetallic catalyst may have the shape of a regular truncated octahedron, it can be asserted that the surface planes are (111) and (100) faces. Then, it is easy to calculate the mean coordination of each site

(vertices, edge, (100) and (111) atoms). Each of these atoms has a coordination number of 6, 7, 8, and 9, respectively. If all the Pd atoms were located at the surface, their total mean coordination number would range between 6 and 9. However, the EXAFS results showed a higher Pd total mean coordination number (around 11). The difference between both coordination numbers is much larger than the precision currently admitted from EXAFS experiments. Then, the probability of a Pd surface segregation does not exist in the $Pd_{16}Co_{84}$/G catalyst.

On the other hand, it is important to stress that EDX analysis on the Pd-Co/G catalysts showed the presence of particles with different palladium and cobalt compositions (17). Small particles were palladium-enriched as the larger ones had a higher cobalt content. Furthermore, XRD results also revealed Pd-Co alloying, but broad diffraction lines suggested that the solid solution was not homogeneous. Mallát *et al*. (13) also suggested the presence of bimetallic particles with heterogeneous composition on carbon-supported Pd-Co catalysts.

Therefore, it can be proposed that the Pd-Co catalysts may be represented by bimetallic particles with different compositions.

4.4. Butadiene Hydrogenation

The addition of cobalt increased the turnover frequencies and influenced product selectivity (Table 4). These results are in good agreement with Sarkany *et al*. (42). According to them, the increase of TOF is not related to the presence of less hydrogen at the surface but instead to a decrease of the adsorption strength of 1,3-butadiene on the Pd sites modified by the second metal.

Sarkany *et al*. (43) also studied the hydrogenation of 1,3-butadiene over Pd/Al_2O_3, Co/Al_2O_3, and $Pd\text{-}Co/Al_2O_3$ catalysts reduced at different temperatures. Independent of the reduction temperature, the *trans/cis* ratio decreased in the following order: $Pd/Al_2O_3 > Pd\text{-}Co/Al_2O_3 > Co/Al_2O_3$. They attributed the behavior of the *trans/cis* ratio to the reduction temperature to the formation of Pd-Co and Co sites. However, it was not possible to determine whether the catalytic and selectivity results were due to electronic effects or selective poisoning of the separate Co sites.

Our activity and selectivity results suggest a modification of the electronic structure of Pd in the presence of Co. Therefore, the formation of a solid solution led to the creation of new sites of Pd-Co, and hence changed the adsorption strength of hydrocarbons, which justifies the activity and selectivity results.

5. CONCLUSIONS

Magnetism, XRD, and EXAFS analyses confirmed the formation of a solid solution on Pd-Co/G catalysts. After reduction at 773 K, XRD results showed the formation of a Pd-Co alloy, but the presence of broad lines suggested that the solid solution was not homogeneous. The magnetic measurements confirmed these results, showing the presence of a Pd-Co alloy with an average composition between rich and poor particles. The EXAFS analysis also revealed the Pd-Co alloying after reduction at 773 K. These results indicated the formation of heterogeneous Pd-Co bimetallic particles. The butadiene hydrogenation suggested a modification of the electronic structure of Pd in the presence of Co. The formation of a solid solution led to the creation of new sites and changed the adsorption strength of hydrocarbons.

ACKNOWLEDGMENTS

F.B.N. is very grateful to CNPq for financial support and the LURE staff for dedicated runs.

REFERENCES

1. Ponec, V., *Catal. Rev. Sci. Eng.* **11**, 41 (1975).
2. Sachtler, W. M. H., and van Santen, R. A., *Adv. Catal.* **26**, 69 (1977).
3. Clarke, J. K. A., *Chem. Rev.* **75**, 291 (1975).
4. Ponec, V., *Adv. Catal.* **32**, 149 (1983).
5. Niemantsverdriet, J. W., Louwers, P. A., van Groudelle, J., van der Kraan, A. M., Kampers, F. W. H., and Koningsberger, D. C., *in* "Proceedings, 9th International Congress on Catalysis, Calgary, 1988" (M. J. Phillips and M. Ternan, Eds.), Vol. 2, p. 674. Chem. Inst. Canada, Ottawa, 1988.
6. Woo, H. S., Fleisch, T. H., Foley, H. C., Uchiyama, S., and Delgass, W. N., *Catal. Lett.* **4**, 93 (1990).
7. Guczi, L., *Catal. Lett.* **7**, 205 (1990).
8. Guczi, L., Hoffer, T., Zsoldos, Z., Zyade, S., Maire, G., and Garin, F., *J. Phys. Chem*. **95**, 802 (1991).
9. Dees, M. J., and Ponec, V., *J. Catal.* **119**, 376 (1989).
10. Mallát, T., Petró, J., Szabó, S., and Sztatisz, J., *React. Kinet. Catal. Lett.* **29**, 353 (1985).
11. Mallát, T., Petró, J., Szabó, S., and Marczis, L., *J. Electroanal. Chem*. **208**, 169 (1986).
12. Mallát, T., Szabó, S., and Petró, J., *J. Acta Chim. Hung.* **124**, 147 (1987).
13. Mallát, T., Szabo, S., Petro, J., Mendioroz, S., and Folgado, M. A., *Appl. Catal.* **53**, 29 (1989).
14. Idriss, H., Diagne, C., Hindermann, J. P., Kinnemann, A., and Barteau, M. A., *in* "Proceedings, 10th International Congress on Catalysis, Budapest, 1992" (L. Guczi, F. Solymosi, and P. Tetenyi, Eds.), Part C, p. 2119. Elsevier, Budapest, 1992.
15. Kapoor, M. P., Lapidus, A. L., and Krylova, A. Y., *in* "Proceedings, 10th International Congress on Catalysis, Budapest, 1992" (L. Guczi, F. Solymosi, and P. Tetenyi, Eds.), Part C, p. 2741. Elsevier, Budapest, 1992.
16. Juszczyk, W., Karpinski, Z., Lomot, D., Pielaszek, J., Paál, Z., and Stakheev, A.Y., *J. Catal*. **142**, 617 (1993).
17. Noronha, F. B., Schmal, M., Nicot, C., Moraweck, B., and Fréty, R., *J. Catal*. **168**, 42 (1997).
18. Dalmon, J. A., *in* "Les Techniques Physiques d'Étude des Catalyseurs" (B. Imelik and J. C. Védrine, Eds.), p. 791. Editions Technip, Paris, 1988.
19. Dalmon, J. A., *J. Catal.* **60**, 325 (1979).
20. Faudon, J. F., Senocq, F., Bergeret, G., Moraweck, B., Clugnet, G., Nicot, C., and Renouprez, A., *J. Catal.* **144**, 460 (1993).
21. Klug, H. P., and Alexander, L. E., "X-Ray Diffraction Procedures for Polycrystalline and Amorphous Materials." Wiley, New York, 1974.
22. Bozorth, R. M., Wolff, P. A., Davis, D. D., Compton, V. B., and Wernick, J. M., *Phys. Rev.* **122**, 1157 (1961).

23. Matsuo, Y., *J. Phys. Soc. Jpn.* **32**, 972 (1972).
24. Moraweck, B., and Renouprez, A. J., *Surf. Sci.* **106**, 35 (1981).
25. Lengeler, B., and Eisenberger, P., *Phys. Rev.* **B21**, 4507 (1980).
26. Nelder, J. A., and Mead, R., *Comp. J.* **7**, 308 (1965).
27. McKale, A. G., Veal, B. W., Paulikas, A. P., Chan, S. K., and Knapp, G. S., *J. Am. Chem. Soc.* **110**, 3763 (1988).
28. Reuel, R. C., and Bartholomew, C. H., *J. Catal.* **85**, 63 (1984).
29. Raab, C., Lercher, J. A., Goodwin, J. G., and Shyu, J., *J. Catal.* **122**, 406 (1990).
30. Sinfelt, J. H., Carter, J. L., and Yates, D. J. C., *J. Catal.* **24**, 283 (1972).
31. Mydosch, J. A., and Nieuwenhuys, G. J., *in* "Ferromagnetic Materials. A Handbook on the Properties of Magnetically Ordered Substances" (E. P. Wolfarth, Ed.), Vol. 1. North Holland, Amsterdam, 1980.
32. Boudart, M., and Hwang, H. S., *J. Catal.* **39**, 44 (1975).
33. Stern, E. A., *Phys. Rev.* **B10**, 3027 (1975).
34. Lytle, F. W., Sayers, D. E., and Stern, E. A., *Phys. Rev.* **B11**, 4825 (1975).
35. Stern, E. A., Sayers, D. E., and Lytle, F. W., *Phys. Rev.* **B11**, 4836 (1975).
36. Sinfelt, J. H., Via, G. H., and Lytle, F. W., *Catal. Rev. Sci. Eng.* **26**, 81 (1984).
37. Bart, J. C. J., and Vlaic, G., *Adv. Catal.* **35**, 1 (1987).
38. van't Blik, H. F. J., Koningsberger, D. C., and Prins, R., *J. Catal.* **97**, 200 (1986).
39. Sinfelt, J. H., Via, G. H., and Lytle, F. W., *J. Chem. Phys.* **72**, 4832 (1983).
40. Tomishige, K., Asakura, K., and Iwasawa, Y., *J. Catal.* **149**, 70 (1994).
41. Ossi, P. M., *Surf. Sci.* **201**, L519 (1988).
42. Sarkany, A., Zsoldos, Z., Furlong, B., Hightower, J. W., and Guczi, L., *J. Catal.* **141**, 566 (1993).
43. Sarkany, A., Zsoldos, Z., Stefler, Gy., Hightower, J. W., and Guczi, L., *J. Catal.* **157**, 179 (1993).